Simple fabrication of AuPd@Pd core-shell nanocrystals for effective catalytic reduction of hexavalent chromium

Fang-Qi Shao, Jiu-Ju Feng, Xiao-Xiao Lin, Liu-Ying Jiang, Ai-Jun Wang*

College of Geography and Environmental Science, College of Chemistry and Life Science, Zhejiang Normal University, Jinhua, 321004, China

ARTICLE INFO

ABSTRACT

Herein, we developed a facile one-pot wet-chemical coreduction method for synthesis of core-shell AuPd@Pd nanocrystals (AuPd@Pd NCs), using polyvinylpyrrolidone (PVP) and minoxidil as the dispersing and growth-directing agents, respectively. The fabricated nanocrystals were mainly characterized by transmission electron microscopy (TEM), scanning transmission electron microscopy (STEM), X-ray photoelectron spectroscopy (XPS) and X-ray diffraction (XRD) in details. The architectures were explored for the catalytic reduction of Cr(VI) to Cr(III) by employing formic acid (HCOOH) as the reducing agent, showing enhanced catalytic activity of AuPd@Pd NCs in contrast with commercial Pd black catalyst. Additionally, the formation mechanism of AuPd@Pd NCs and the catalytic reduction mechanism of Cr(VI) were illustrated and discussed in some detail, respectively.

© 2017 Elsevier B.V. All rights reserved.

1. Introduction

Chromium generally exists in the two oxidation states of hexavalent chromium (Cr(VI)) and trivalent chromium (Cr(III)) in environment. The former is well-known as one of the most common pollutants, which is proved to have mutagenicity, acute toxicity, carcinogenicity, and high environmental mobility [1,2]. However, the latter is considered as an essential nutrient required for human and animal, which is much less soluble in water and less toxic to human [3,4]. Therefore, it is necessary to remediate Cr(VI) contamination from environment to avoid Cr(VI) induce severe environmental and health problems.

Recently, many feasible methods have been developed to remove Cr(VI) from environment, including chemical precipitation [5], solvent extraction [6], ion exchange [7], membrane processes [8], and biological process [9]. However, most of these involve high cost and time-consuming progresses, which also depend by many experimental parameters such as the mixing time, pH and precipitation agent [10,11].

Remarkably, it is reasonable to overcome Cr(VI) contamination by the reduction of Cr(VI) to Cr(III) with different materials and compounds, including seabacterium strain [12], hydrogen sulfide [13], sodium dithionite ($Na_2S_2O_4$) [14], and Fe(II) [15]. Recently, noble metals (e.g., Pd, Pt, Ag, and Au) have received significant

attention for Cr(VI) reduction [16]. For example, Fu et al. synthesized Pd tetrapods in the reduction of Cr(VI) with formic acid [17]. Marcell et al. prepared Pd nanoparticles (NPs) to reduce Cr(VI) in the presence of formic acid [18]. These successful examples strongly demonstrate Pd NPs as an effective catalyst for environmental remediation of Cr(VI).

Bimetallic noble metals with hetero- [19], alloy- [20] and core-shell [21] nanostructures have attracted tremendous interest for their improved catalytic performances, owing to their bifunctional and/or synergistic effects [22]. Among them, Pd-based nanomaterials are widely explored as nanocatalysts, thanks to their low cost but high catalytic activity and stability when compared with monometallic counterparts [23].

Many Pd-based core-shell nanocrystals (NCs) with superior catalytic activity have been constructed [24]. Li et al. prepared Pt@Pd core-shell nanowires by a multi-step method with Pd nanowires as the intermediate [25]. Huang's group fabricated Au@Pd heterostructures by the seed-mediated method to grow a Pd shell on a Au nanocrystal core [26]. However, the complicated fabrication steps usually make their synthesis complicated and time-consuming [27], which further confine their large-scaled preparation.

It is feasible for simple and shape-controlled synthesis of Pd-based multinary NCs by virtue of a novel growth-directing agent. Lately, a seedless one-step co-reduction method was developed to fabricate AuPd@Pd NCs [28] and AuPd@Pd NCs/graphene [29] by using allantoin and 4-(2-hydroxyethyl)-1-piperazineethane- sulfonic acid as the shaping-directing agents, respectively.

* Corresponding author.
  E-mail addresses: ajwang@zjnu.cn, ajwangnju@gmail.com (A.-J. Wang).

As an orally administered antihypertensive agent, minoxidil (6-(1-piperidinyl)-2,4-pyrimidinediamine-3-oxide, Fig. S1, Supporting Information, SI) is nontoxic and usually used in male-pattern baldness, hypertrichosis and hypertension [30]. Herein, a facile one-pot aqueous method was developed to construct core-shell AuPd@Pd NCs by using minoxidil as a new growth-directing agent. The catalytic activity, stability and reusability of the prepared AuPd@Pd NCs were examined by the catalytic reduction of Cr(VI) with formic acid in details.

2. Experimental

2.1. Synthesis of AuPd@Pd NCs

In a typical process, 0.0534 g of minoxidil (25 mmol L^{-1}) was firstly dissolved with 2.577 mL of water and 0.400 mL of 0.5 mol L^{-1} H$_2$SO$_4$. Next, 0.823 mL of HAuCl$_4$, 0.200 mL of H$_2$PdCl$_4$ and 5 mL of PVP (1.0 wt.%) were subsequently put into the above mixed solution. Afterward, 1.0 mL of the freshly-prepared ascorbic acid (AA, 0.1 mol L^{-1}) was slowly injected into the mixture and reacted for 2.5 h under stirring at 60 °C, with the color gradually changing from initial orange to brown. Herein, AA acts as a reducing agent to reduce the precursors (AuCl$_4^-$ and PdCl$_4^{2-}$). The resulting product was collected by centrifugation (12,000 rpm, 5 min), thoroughly purifying with water, and finally drying in vacuum at 60 °C.

Controlled experiments were conducted with different amounts of minoxidil (5, 10, and 50 mmol L^{-1}), while the other experimental parameters were kept the same.

2.2. Catalytic reduction of Cr(VI)

Herein, AuPd@Pd NCs were examined as a catalyst to accelerate the reduction reaction of Cr(VI) by formic acid. Typically, 0.6 mL of the AuPd@Pd NCs suspension (1.0 mg mL^{-1}) was put into the mixture containing 7.4 mL water, 1.0 mL of postassium dichromate (K$_2$Cr$_2$O$_7$, 50 mmol L^{-1}) and 1.0 mL of formic acid (88 wt.%) under stirring at 50 °C. At each predetermined interval, 180.0 μL of the mixed solution was withdrawn and diluted to 3 mL, followed by recording the corresponding UV–vis spectra on a UV–vis absorp-tion spectrometer to detect the remained Cr(VI) concentration until the mixture color turned from yellow to colorless. For comparison, controlled experiments were conducted without catalysts or using commercial Pd-black and AuPd NCs (prepared without minoxidil) as the referenced catalysts under the same experimental condi-tions.

In the recycle experiments, 1.0 mL of the K$_2$Cr$_2$O$_7$ solution (50 mmol L^{-1}) and 1 mL formic acid (88%) were mixed with 7.4 mL of water, followed by injecting 0.6 mL of the AuPd@Pd NCs suspen-sion (1.0 mg mL^{-1}) to initiate the reaction. After the first reaction cycle, another certain amount of K$_2$Cr$_2$O$_7$ solution was dropped into the mixture again to continue the recycle test. Remarkably, the amount of K$_2$Cr$_2$O$_7$ solution introduced to the reaction system is different for each cycle because of the withdrawn mixture. How-ever, it is essential to keep the fixed K$_2$Cr$_2$O$_7$ concentration (i.e., 5.0 mmol L^{-1}) at the initial state before each cycle.

More detailed information of *Materials* and *Characterization* were provided in Supporting Information (SI).

3. Results and discussion

3.1. Physicochemical characterization

The structure and morphology of the typical product were char-acterized by transmission electron microscopy (TEM) and high resolution TEM (HRTEM) measurements. As illustrated in Fig. 1A and B, there are many well-dispersed and uniform flower-like nanostructures observed, with an average diameter of 52.5 nm (inset in Fig. 1A). Furthermore, Fig. 1C–E shows the HRTEM images of the as-prepared nanocrystals, in which the lattice fringes can be easily measured to be 0.225 and 0.224 nm, originating from the (111) crystal planes of the face-centered cubic (fcc) Pd [31]. Besides, the selected area electron diffraction (SAED) pattern exhibits con-tinuous diffraction rings from inner to outside, suggesting the polycrystalline nature of AuPd@Pd NCs (inset in Fig. 1B) [28].

High-angle annular dark-field scanning transmission electron microscopy-energy dispersive X-ray spectrometer (HAADF-STEM-EDS) experiments were conducted to investigate the elemental distribution of the as-prepared nanocrystals (Fig. 2). The corre-
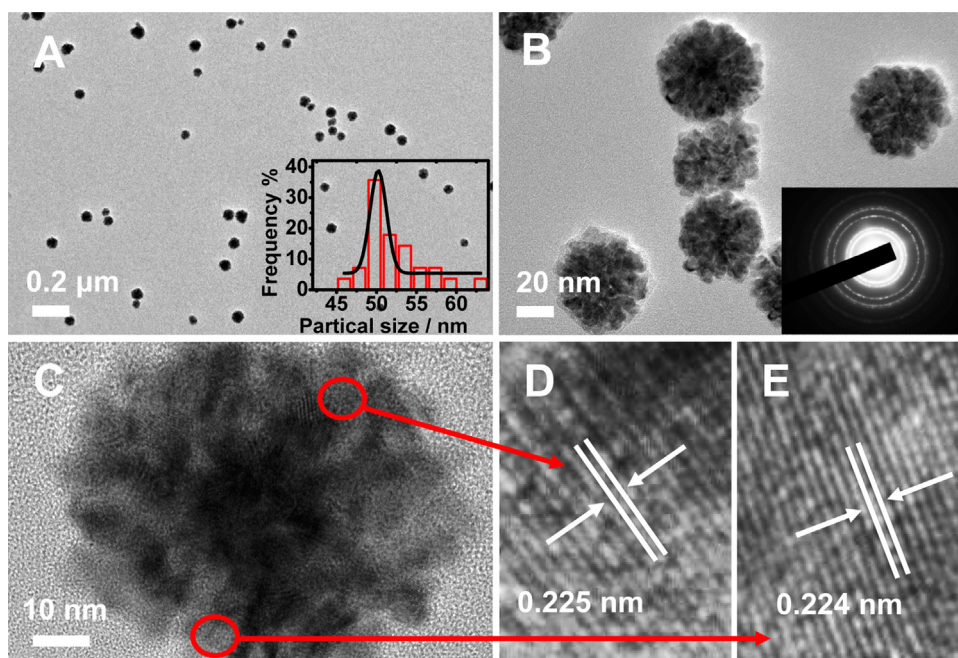

Fig. 1. TEM (A, B, C) and HR-TEM (D, E) images of AuPd@Pd NCs. Insets in (A) and (B) show the corresponding particle-size distribution and the SAED pattern, respectively.
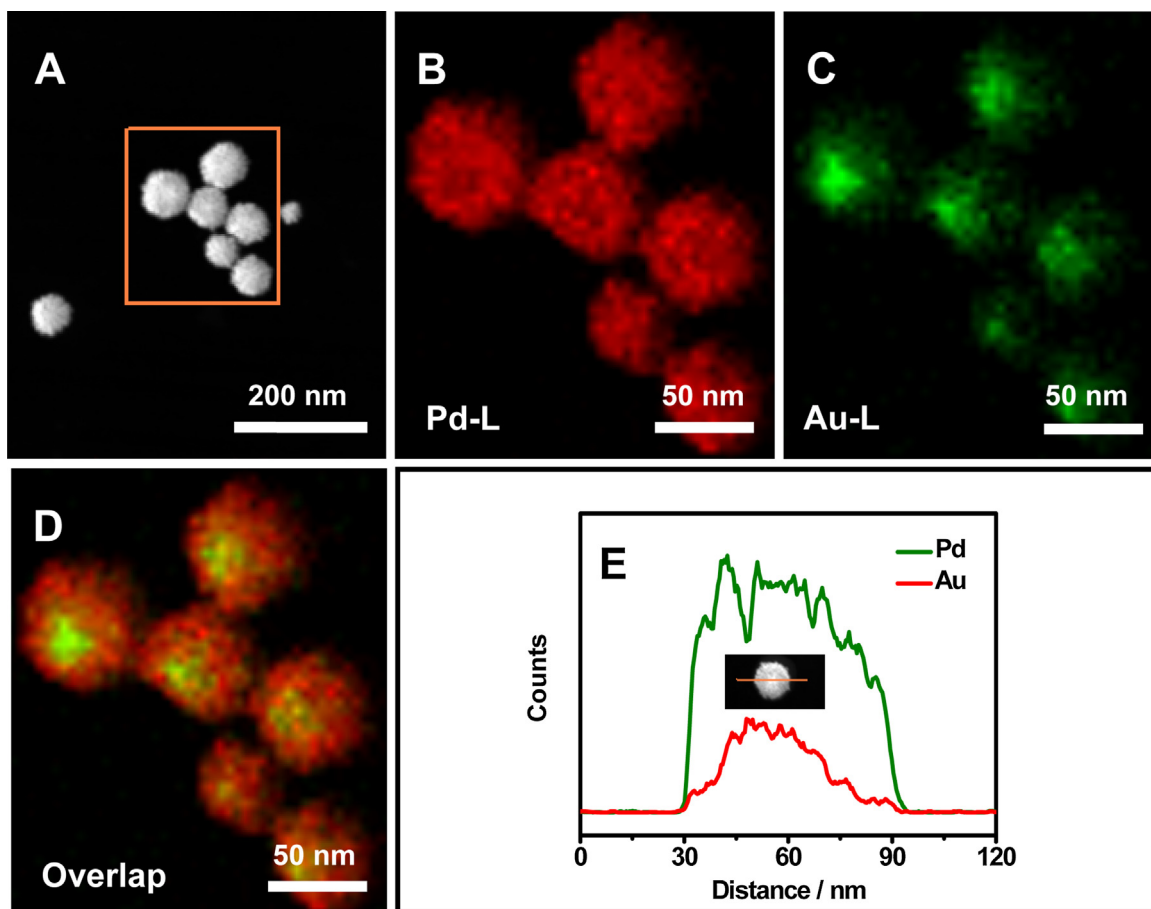
Fig. 2. HAADF-STEM image (A), HAADF-STEM-EDS elemental mapping images of individual Pd (B), Au (C), and overlap (D), cross-sectional compositional line scanning profiles (E) of a single AuPd@Pd nanocrystal.

sponding EDS mapping images reveal that Au element is mainly detected in the center (Fig. 2B), while Pd element is uniformly distributed throughout the whole nanocrystals (Fig. 2C), strongly showing the formation of the core-shell structures. This assumption is supported by the line scanning profiles, showing the coexistence of Pd and Au atoms as the core, whereas only Pd atoms emerge in the external shell (Fig. 2E).

X-ray photoelectron spectroscopy (XPS) measurements were performed to identify the compositions and chemical valence states of AuPd@Pd NCs. As depicted by the high-resolution Au 4f XPS spectrum (Fig. 3A), a pair of peaks shows up at 83.80 eV (Au $4f_{7/2}$) and 87.51 eV (Au $4f_{5/2}$), which are attributed to metallic Au^0, suggesting the efficient reduction of $AuCl_4^-$ [32]. Besides, the associated Pd 3d peak (Fig. 3B) exhibit two pairs of peaks detected at 340.23 eV (Pd $3d_{3/2}$) and 334.93 eV (Pd $3d_{5/2}$); 342.00 eV (Pd $3d_{3/2}$) and 337.11 eV (Pd $3d_{5/2}$), corresponding to Pd^0 and Pd^{2+} species, indicating that metallic Pd^0 is the main species, showing the complete reduction of $PdCl_4^{2-}$ [33]. As calculated by the XPS analysis, the contents of Pd^0 and Pd^{2+} are 94.89% and 5.11%, respectively, further revealing that metallic Pd^0 is the main species.

The crystal structure of AuPd@Pd NCs was determined by X-ray diffraction (XRD). As seen in Fig. 4, the representative diffraction peaks detected at 38.2°, 44.5°, 64.8°, 77.7°, and 82.0° are well indexed to the (111), (200), (220), (311) and (222) facets of the fcc AuPd alloy [28], respectively. Meanwhile, the diffraction peaks all consistently emerge between those of bulk Au and Pd, which confirms the formation of the AuPd alloy [34]. Besides, the weak shoulder peak appeared from each peak indicate the emergence
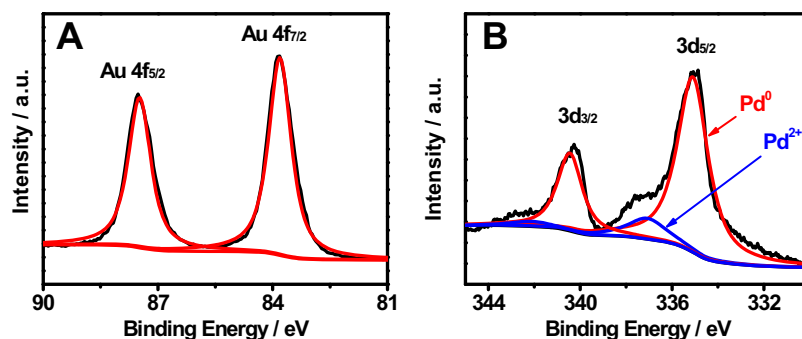

Fig. 3. (A, B) High-resolution (A) Au 4f and (B) Pd 3d XPS spectra of AuPd@Pd NCs.
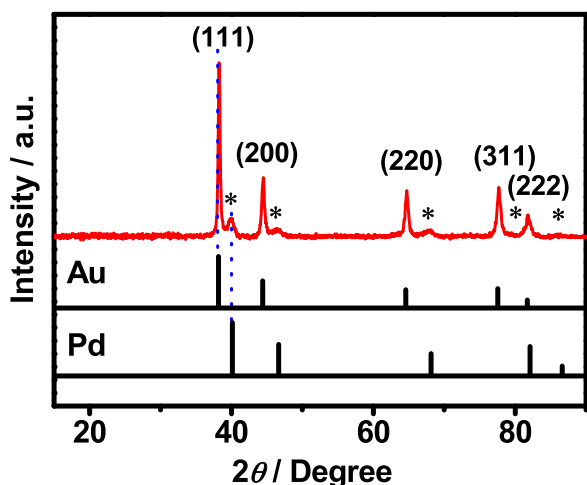
Fig. 4. XRD pattern of AuPd@Pd NCs. The standard XRD spectra of pure Au (JCPDS 04-0784) and Pd (JCPDS 46-1043) are shown for comparison.

of the external Pd shell around the AuPd core, powerfully demonstrating the formation of the core-shell AuPd@Pd structures again [28].

3.2. Formation mechanism

In this work, a one-step minoxidil-assisted aqueous strategy was designed for synthesis of AuPd@Pd NCs at 60 °C within 2.5 h. In control experiments, we further investigated the effects of the minoxidil concentrations on the final products. As displayed by the TEM images (Fig. 5A), many irregular nanoparticles show up in the absence of minoxidil. Besides, insufficient (e.g., 5 and 10 mmol L^{-1}) minoxidil induces the formation of many large irregular nanocrystals with aggregation. Alternatively, excess minoxidil (e.g., 50 mmol L^{-1}) yields much small nanocrystals without any specific morphology (Fig. 5D). These observations demonstrate the

essential role of minoxidil as a structure director in the current synthesis.

In another control experiment (Fig. S2A, SI), the absence of PVP induces the formation of the final AuPd product with heavy aggregation. Therefore, the existence of PVP can efficiently prevent the synthesized nanocrystals from aggregation, which serves as a dispersing agent in the synthetic process.

Taken together, Fig. 6 illustrates the formation mechanism of AuPd@Pd NCs. Firstly, the reduction of AuCl$_4^-$ is much easier when compared with that of PdCl$_4^{2-}$ in the presence of minoxidil and PVP, because of the higher reduction potential of AuCl$_4^-$/Au (1.002 V vs. RHE) than PdCl$_4^{2-}$/Pd (0.591 V vs. RHE) [28]. The metal precursors (AuCl$_4^-$ and PdCl$_4^{2-}$) are firstly reduced to Au and Pt atoms after the addition of AA, which are quickly covered by the adjacent minoxidil molecules. The as-formed Au and Pd nuclei continuously aggregate together to minimize the total surface energy [35], resulting in the formation of the spherical particles. Herein, minoxidil molecules have selective adsorption ability on specific crystal planes to direct the final morphologies, leading to the formed AuPd nuclei preferentially grow along the (111) planes to form AuPd alloyed nanostructures. Meanwhile, PVP acts as the dispersing agent to effectively disperse the particles. After the complete consumption of AuCl$_4^-$, the residual PdCl$_4^{2-}$ continually reduces to generate the external Pd shell around AuPd nuclei via the crystal over-growth to eventually form AuPd@Pd NCs.

3.3. Catalytic tests

The catalytic activity of AuPd@Pd NCs was studied by the reduction of Cr(VI) with formic acid which attracts significant interest as a reducing agent for its reduction of Cr(VI) and direct decomposition to carbon dioxide (CO$_2$) and hydrogen (H$_2$) with the assistance of metal catalysts [36]. For the chemical decomposition of formic acid, the dehydrogenation pathway (HCOOH → CO$_2$ + H$_2$) and dehydration pathway (HCOOH → CO + H$_2$O) are generally two kinds of pathways occurred [17], which are mainly dependent by
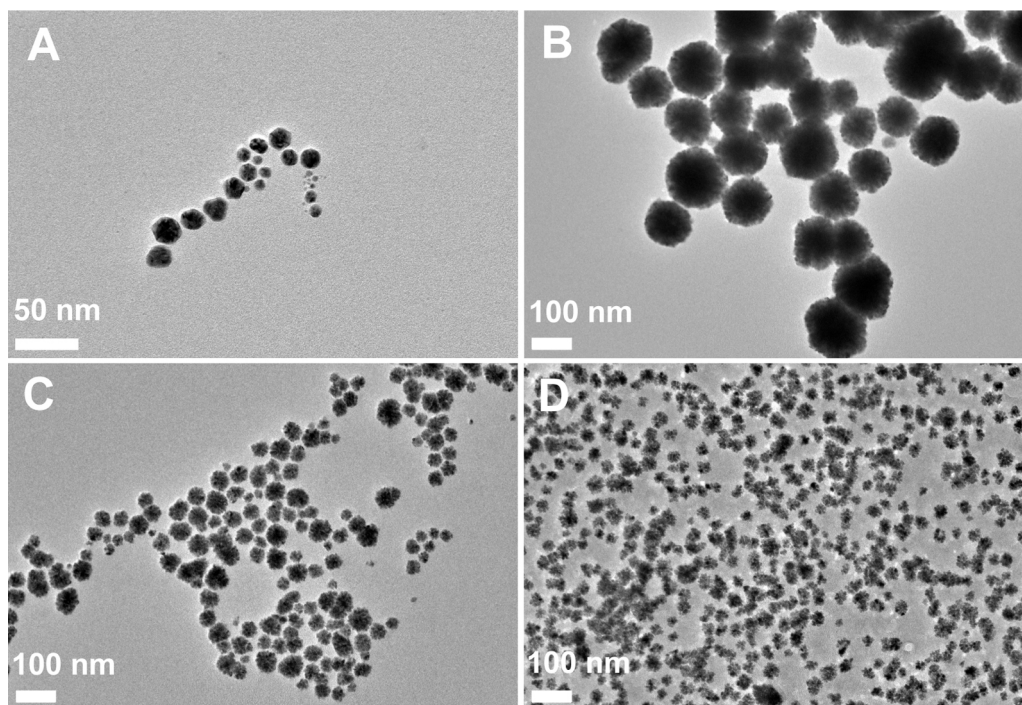

Fig. 5. TEM images of the AuPd products obtained without (A), with 5 mmol L^{-1} (B), 10 mmol L^{-1} (C), and 50 mmol L^{-1} (D) minoxidil.
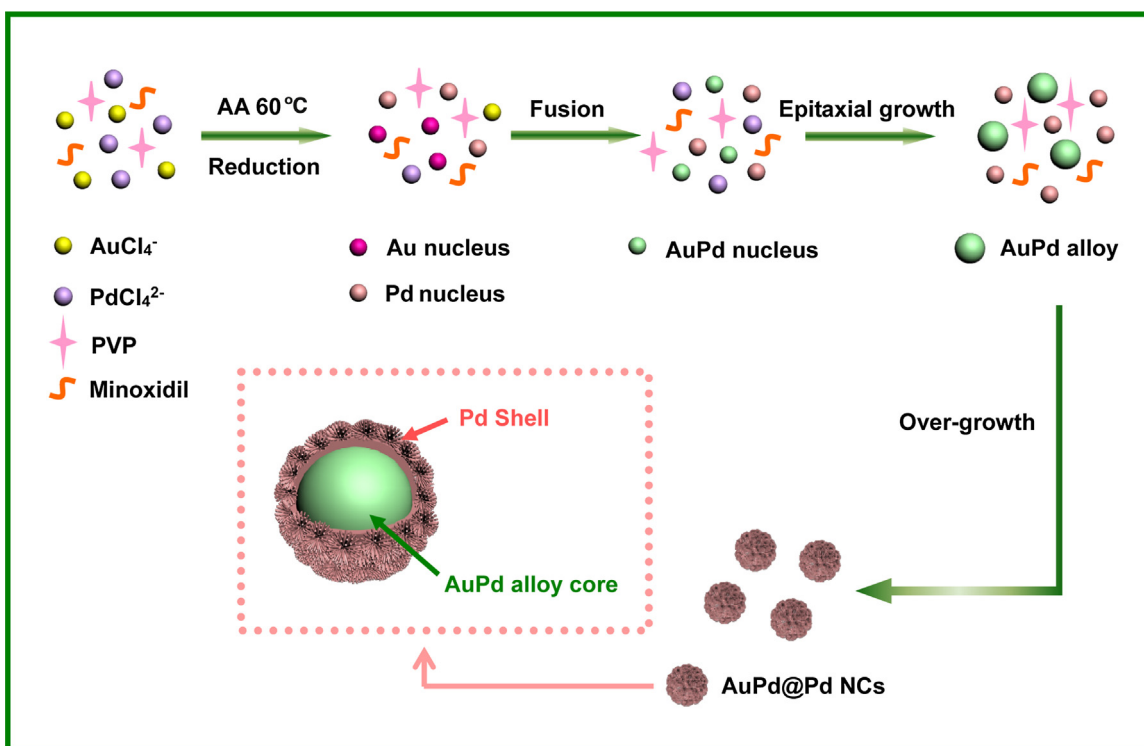
Fig. 6. Schematic illustration of the formation mechanism of AuPd@Pd NCs.

the catalysts, pH values and reaction temperature in the system [37–39].

Besides, when the decomposition process is occurred on the Pd (111) planes, there is more prominent tendency to transform through dehydrogenation pathway rather than dehydration pathway, due to the much low barrier for dehydrogenation pathway [40,41]. As described by Fig. 7, formic acid is degraded to CO_2 and H_2 only in the presence of AuPd@Pd NCs via the dehydrogenation pathway, followed by the transformation of Cr(VI) to Cr(III) by virtue of the generated H_2.

UV–vis absorption spectroscopy measurements were performed to monitor the reduction reaction processes. The characteristic absorbance of Cr(VI) is located at 350 nm, which is originated from the ligand (oxygen) to metal (Cr(VI)) charge transfer (LMCT) [42,43]. As shown in Fig. 8A–C, the absorbance intensities of Cr(VI) decrease successively after the introduction of AuPd@Pd NCs (A), using commercial Pd black (B) and AuPd NCs (prepared without minoxidil, C) as the references. The corresponding catalytic activities are visually confirmed by the variation rate in the solution color typically from yellow to colorless. Besides, the
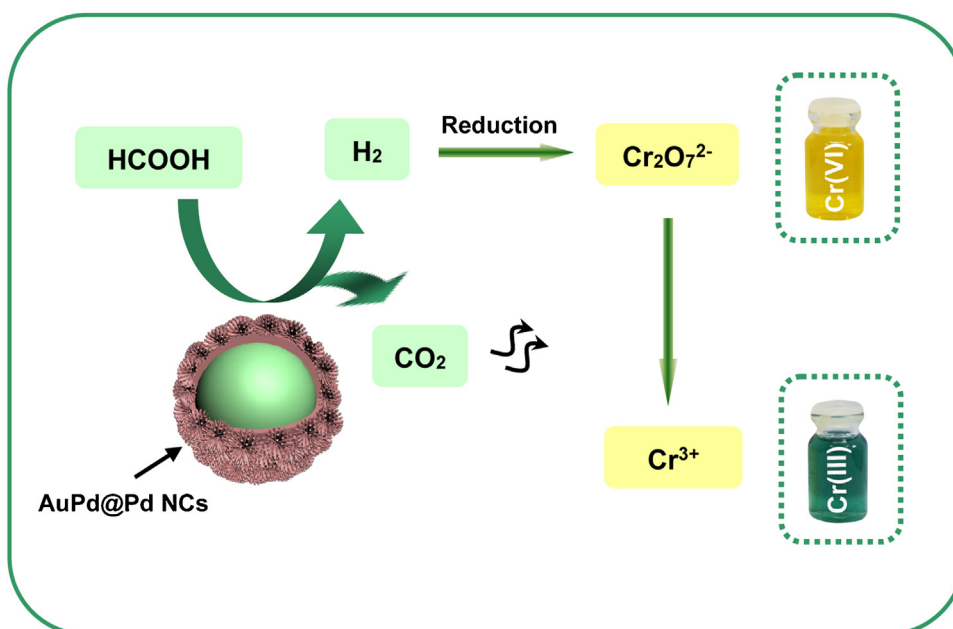

Fig. 7. Schematic illustration of the catalytic reduction of Cr(VI) on AuPd@Pd NCs.
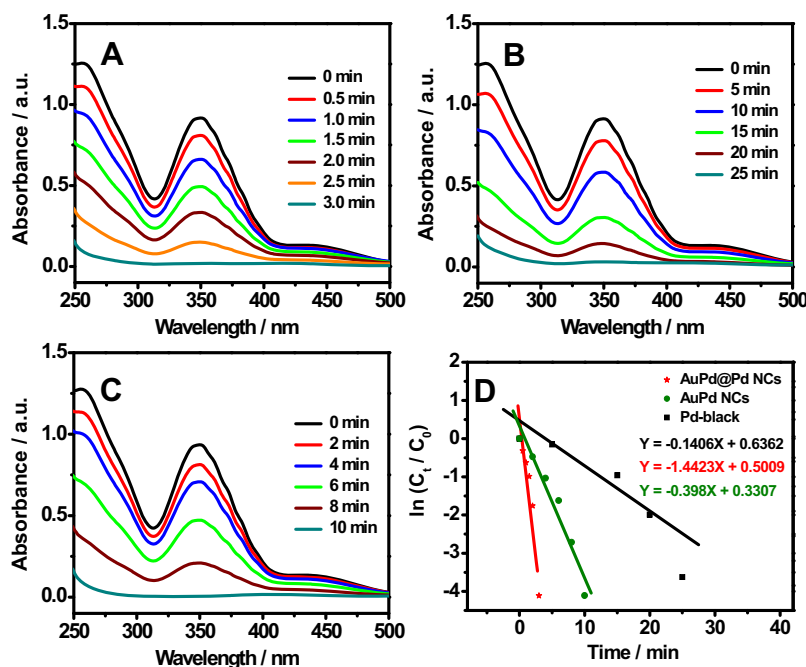
Fig. 8. UV–vis spectra of Cr(VI) recorded from the aqueous media in the presence of formic acid at 50 °C treated with (A) AuPd@Pd NCs, (B) Pd black, and (C) AuPd NCs prepared without minoxidil. (D) The relationship between the ln (C_t/C_0) and reaction time (t).

presence of Cr(III) is confirmed by putting sufficient NaOH into the reaction system, accompanied with the color change from colorless to green. It indicates the generation of hexahydroxochromate(III) [18,44], as vividly illustrated in Fig. 7.

As revealed in Fig. 8A, the absorbance at 350 nm disappears within 3 min after the introduction of a certain amount of AuPd@Pd NCs, thanks to the complete reduction of the initial Cr(VI) species. However, 25 and 10 min are required to complete the reduction by using commercial Pd black (Fig. 8B) and AuPd NCs prepared without minoxidil (Fig. 8C), respectively, which are 3.33- and 8.33-fold longer than that of AuPd@Pd NCs under the same conditions. It means much higher catalytic activity of AuPd@Pd NCs [17,43,45]. Furthermore, the absorbance intensity of Cr(VI) slightly decreases within 30 min in the absence of any catalyst (Fig. S3, SI), showing the indispensable role of the catalyst for the Cr(VI) reduction.

The reaction kinetics are commonly determined to further evaluate the catalytic performance of catalysts [17], as typically described as $-ln(C_t/C_0) = \kappa t$. The kinetic rate constant (κ) is calculated from the slope of the linear plot, t is the reaction time, C_0 and C_t are the concentrations of Cr(VI) in the reaction solution at the initial and time t, respectively. Evidently, the κ is calculated to be 1.4423 min^{-1} for AuPt@Pd NCs (Fig. 8D), which is much higher than those for Pd black (0.1406 min^{-1}) and AuPd NCs without minoxidil (0.3980 min^{-1}), indicating the better catalytic activity of AuPd@Pd NCs for the reduction of Cr(VI) [17].

Table S1 (SI) shows the comparison of AuPd@Pd NCs with the other nanocatalysts for the catalytic reduction of Cr(VI). Clearly, the catalytic activity of the AuPd@Pd NCs catalyst is much higher than those of Pd NPs@pro-ESM [16], Pd NPs@NIL-101 [36], Pd NPs-immobilized PEI/PVA [43], Pd@SiO$_2$-NH$_2$ [46], Pd-Cu nanospheres [47], and Pd nanowires networks [48], and comparable with those of Pd tetrapods [17] and Pd nanoparticles [18]. These results demonstrate AuPd@Pd NCs have highly catalytic activity for the catalytic reduction of Cr(VI).

Recycle experiments were conducted to investigate the stability and reusability of the as-prepared AuPd@Pd NCs. As shown in Fig. 9, the as-synthesized AuPd@Pd NCs still have high catalytic efficiency and almost constant response time even after 12 cycles in contrast
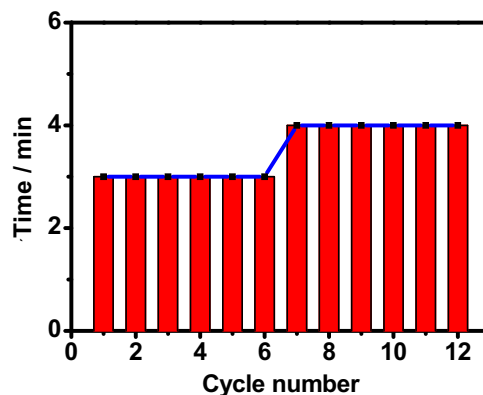

Fig. 9. The recycle test of AuPd@Pd NCs in the presence of formic acid.

with the initial values, confirming the excellent reusability of the catalyst [43]. Besides, the negligible deterioration of the catalyst after each cycle is ascribed to the formation of palladium hydride (PdH$_x$) species on AuPd@Pd NCs originated from the newly-formed H$_2$ by the decomposition of formic acid [49].

The improved catalytic activity and stability of AuPd@Pd NCs towards the Cr(VI) reduction are attributed to the following aspects: (i) The synergetic electronic effects between Pd and Au effectively improve the catalytic performances [50]. (ii) The special flower-like nanocrystals with multi-branches provide enlarged active surface area [51]. (iii) The specific Pd shells offer more active sites available for the catalytic reduction of Cr(VI) [52].

4. Conclusions

In summary, a facile one-pot aqueous coreduction method was developed for the synthesis of AuPd@Pd NCs by using minoxidil and PVP as the structure director and dispersing agent, respectively, without any organic solvent, template or premade seed. The architectures exhibit enhanced catalytic activity for the reduction of Cr(VI) with a higher reaction kinetics as compared with Pd black

and AuPd NCs (prepared without minoxidil) under the identical conditions. Furthermore, the as-synthesized nanocatalyst is easily to be recycled for at least 12 times with similar performances, showing the superior reusable ability. These results demonstrate AuPd@Pd NCs as a promising catalyst in environmental remediation. Moreover, this synthetic route provides new insights for fabricating other nanocatalysts in the environmental remediation processes.

Acknowledgement

Appendix A. Supplementary data

Supplementary data associated with this article can be found, in the online version, at http://dx.doi.org/10.1016/j.apcatb.2017.02.051.

References

[1] D.W. Elliott, W.-X. Zhang, Environ. Sci. Technol. 35 (2001) 4922–4926.
[2] D.M. Stearns, L.J. Kennedy, K.D. Courtney, P.H. Giangrande, L.S. Phieffer, K.E. Wetterhahn, Biochemistry 34 (1995) 910–919.
[3] H. Kyung, J. Lee, W. Choi, Environ. Sci. Technol. 39 (2005) 2376–2382.
[4] A. Zhitkovich, Chem. Res. Toxicol. 24 (2011) 1617–1629.
[5] M.F. Almeida, R.A. Boaventura, Waste Manage. 17 (1998) 201–209.
[6] P. Venkateswaran, K. Palanivelu, Sep. Purif. Technol. 40 (2004) 279–284.
[7] S. Kocaoba, G. Akcin, Talanta 57 (2002) 23–30.
[8] A. Hafez, M. El-Manharawy, M. Khedr, Desalination 144 (2002) 237–242.
[9] Z.A. Zakaria, Z. Zakaria, S. Surif, W.A. Ahmad, J. Hazard. Mater. 146 (2007) 30–38.
[10] M.A. Chaudry, S. Ahmad, M.T. Malik, Waste Manage. 17 (1998) 211–218.
[11] V.A. Okello, S. Mwilu, N. Noah, A. Zhou, J. Chong, M.T. Knipfing, D. Doetschman, O.A. Sadik, Environ. Sci. Technol. 46 (2012) 10743–10751.
[12] A. Shakoori, M. Makhdoom, R. Haq, Appl. Microbiol. Biotechnol. 53 (2000) 348–351.
[13] E.C. Thornton, J.E. Amonette, Environ. Sci. Technol. 33 (1999) 4096–4101.
[14] J.S. Fruchter, C.R. Cole, M.D. Williams, V.R. Vermeul, J.E. Amonette, J.E. Szecsody, J.D. Istok, M.D. Humphrey, Ground Water Monit. Rem. 20 (2000) 66–77.
[15] D.L. Sedlak, P.G. Chan, Geochim. Cosmochim. Acta 61 (1997) 2185–2192.
[16] M. Liang, R. Su, W. Qi, Y. Zhang, R. Huang, Y. Yu, L. Wang, Z. He, Ind. Eng. Chem. Res. 53 (2014) 13635–13643.
[17] G.-T. Fu, X. Jiang, R. Wu, S.-H. Wei, D.-M. Sun, Y.-W. Tang, T.-H. Lu, Y. Chen, ACS Appl. Mater. Interfaces 6 (2014) 22790–22795.
[18] M.A. Omole, I.O. K'Owino, O.A. Sadik, Appl. Catal. B: Environ. 76 (2007) 158–167.
[19] Z. Peng, H. Yang, J. Am. Chem. Soc. 131 (2009) 7542–7543.
[20] S. Zhang, Y. Shao, H.-g. Liao, J. Liu, I.A. Aksay, G. Yin, Y. Lin, Chem. Mater. 23 (2011) 1079–1081.
[21] L. Wang, Y. Yamauchi, J. Am. Chem. Soc. 132 (2010) 13636–13638.
[22] D. Wang, Y. Li, Adv. Mater. 23 (2011) 1044–1060.
[23] F. Yu, W. Zhou, R.M. Bellabarba, R.P. Tooze, Nanoscale 6 (2014) 1093–1098.
[24] M.B. Gawande, A. Goswami, T. Asefa, H. Guo, A.V. Biradar, D.-L. Peng, R. Zboril, R.S. Varma, Chem. Soc. Rev. 44 (2015) 7540–7590.
[25] H.-H. Li, S.-Y. Ma, Q.-Q. Fu, X.-J. Liu, L. Wu, S.-H. Yu, J. Am. Chem. Soc. 137 (2015) 7862–7868.
[26] C.-W. Yang, K. Chanda, P.-H. Lin, Y.-N. Wang, C.-W. Liao, M.H. Huang, J. Am. Chem. Soc. 133 (2011) 19993–20000.
[27] F.-R. Fan, D.-Y. Liu, Y.-F. Wu, S. Duan, Z.-X. Xie, Z.-Y. Jiang, Z.-Q. Tian, J. Am. Chem. Soc. 130 (2008) 6949–6951.
[28] Q. Liu, Y.-R. Xu, A.-J. Wang, J.-J. Feng, Int. J. Hydrogen Energy 41 (2016) 2547–2553.
[29] J.-N. Zheng, S.-S. Li, X. Ma, F.-Y. Chen, A.-J. Wang, J.-R. Chen, J.-J. Feng, J. Power Sources 262 (2014) 270–278.
[30] R.C. Wester, H.I. Maibach, R.H. Guy, E. Novak, J. Invest. Dermatol. 82 (1984) 515–517.
[31] G. Fu, Z. Liu, Y. Chen, J. Lin, Y. Tang, T. Lu, Nano Res. 7 (2014) 1205–1214.
[32] F. Li, Y. Guo, R. Li, F. Wu, Y. Liu, X. Sun, C. Li, W. Wang, J. Gao, J. Mater. Chem. A 1 (2013) 6579–6587.
[33] G. Fu, K. Wu, J. Lin, Y. Tang, Y. Chen, Y. Zhou, T. Lu, J. Phys. Chem. C 117 (2013) 9826–9834.
[34] Z. Li, R. Li, T. Mu, Y. Luan, Chem. Eur. J. 19 (2013) 6005–6013.
[35] L. Liu, X.-X. Lin, S.-Y. Zou, A.-J. Wang, J.-R. Chen, J.-J. Feng, Electrochim. Acta 187 (2016) 576–583.
[36] M. Yadav, Q. Xu, Chem. Commun. 49 (2013) 3327–3329.
[37] S. Enthaler, J. von Langermann, T. Schmidt, Energy Environ. Sci. 3 (2010) 1207–1217.
[38] B. Loges, A. Boddien, F. Gärtner, H. Junge, M. Beller, Top. Catal. 53 (2010) 902–914.
[39] M. Yadav, Q. Xu, Energy Environ. Sci. 5 (2012) 9698–9725.
[40] K. Mori, M. Dojo, H. Yamashita, ACS Catal. 3 (2013) 1114–1119.
[41] R. Zhang, H. Liu, B. Wang, L. Ling, J. Phys. Chem. C 116 (2012) 22266–22280.
[42] J.B. Chlistunoff, K.P. Johnston, J. Phys. Chem. B 102 (1998) 3993–4003.
[43] Y. Huang, H. Ma, S. Wang, M. Shen, R. Guo, X. Cao, M. Zhu, X. Shi, ACS Appl. Mater. Interfaces 4 (2012) 3054–3061.
[44] A. Esmaeili, R. Vazirinejad, Am. J. Appl. Sci. 2 (2005) 1471–1473.
[45] O.A. Sadik, N.M. Noah, V.A. Okello, Z. Sun, J. Chem. Educ. 91 (2013) 269–273.
[46] M. Celebi, M. Yurderi, A. Bulut, M. Kaya, M. Zahmakiran, Appl. Catal. B: Environ. 180 (2016) 53–64.
[47] S.-H. Han, J. Bai, H.-M. Liu, J.-H. Zeng, J.-X. Jiang, Y. Chen, J.-M. Lee, ACS Appl. Mater. Interfaces 8 (2016) 30948–30955.
[48] L.-L. Wei, R. Gu, J.-M. Lee, Appl. Catal. B: Environ. 176–177 (2015) 325–330.
[49] T.-H. Phan, R.E. Schaak, Chem. Commun. (2009) 3026–3028.
[50] F. Gao, D.W. Goodman, Chem. Soc. Rev. 41 (2012) 8009–8020.
[51] S.-S. Li, A.-J. Wang, Y.-Y. Hu, K.-M. Fang, J.-R. Chen, J.-J. Feng, J. Mater. Chem. A 2 (2014) 18177–18183.
[52] Z. Dong, X. Le, C. Dong, W. Zhang, X. Li, J. Ma, Appl. Catal. B: Environ. 162 (2015) 372–380.